# Dual structure of a vanadyl-based molecular qubit containing a bis(β-diketonato) ligand

Manuel Imperato,[a,b,#] Alessio Nicolini,[a,#] Matteo Boniburini,[a] Daniele Sartini,[c] Enrico Benassi,[b] Mario Chiesa,[d] Lara Gigli,[e] Yu-Kai Liao,[d] Arsen Raza,[c] Enrico Salvadori,[d] Lorenzo Sorace,[c] and Andrea Cornia[a,*]

[a]Dipartimento di Scienze Chimiche e Geologiche e UdR INSTM, Università degli Studi di Modena e Reggio Emilia, via G. Campi 103, 41125 Modena, Italy. E-mail: acornia@unimore.it

[b]Dipartimento di Scienze Fisiche, Informatiche e Matematiche, Università degli Studi di Modena e Reggio Emilia, via G. Campi 213/A, 41125 Modena, Italy

[c]Dipartimento di Chimica "Ugo Schiff" e UdR INSTM, Università degli Studi di Firenze, via della Lastruccia 3, 50019 Sesto Fiorentino (FI), Italy

[d]Dipartimento di Chimica e NIS Centre, Università degli Studi di Torino, via P. Giuria 7, 10125 Torino, Italy

[e]Elettra-Sincrotrone Trieste S.C.p.A., Strada Statale 14 - km 163.5 in AREA Science Park, 34149 Basovizza (TS), Italy

## SUPPORTING INFORMATION

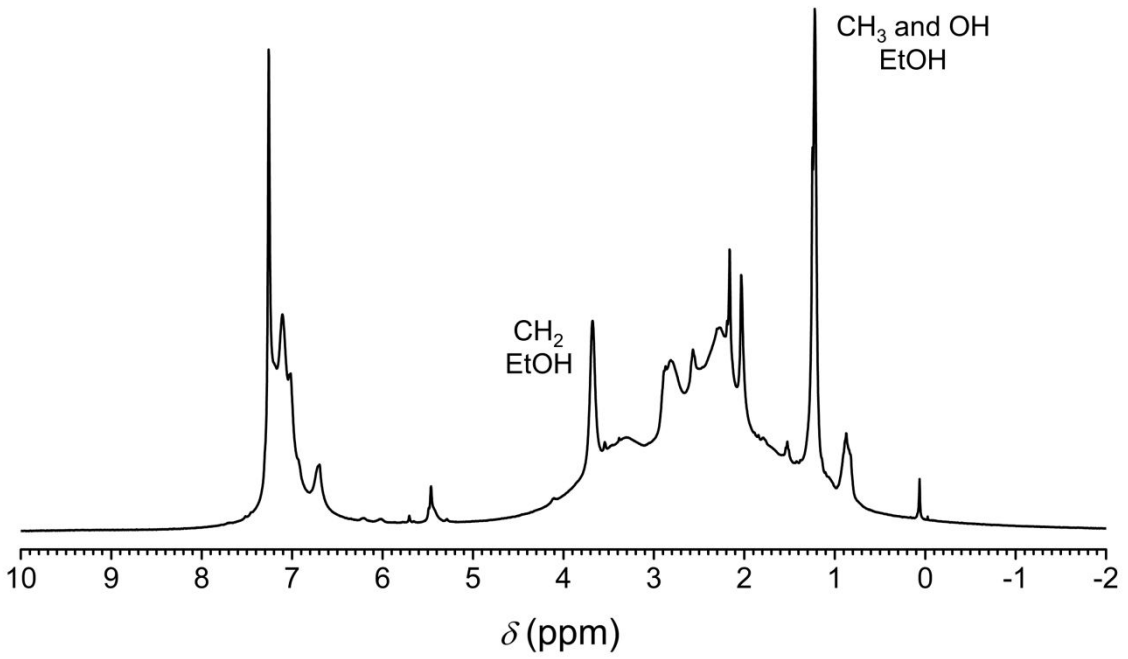


**Figure S1.** $^{1}$H-NMR spectrum of the crude VO(bdhb)$(EtOH)_{0.35}(H_2O)_{0.35}$ material in $CDCl_3$ (400.13 MHz, 298 K). The main narrow peaks are from EtOH (3.68 and 1.22 ppm) and residual proton impurities in the solvent (7.26 ppm). Processing parameters (TopSpin 4.3.0[1]): SI = TD, LB = 1.00 Hz.

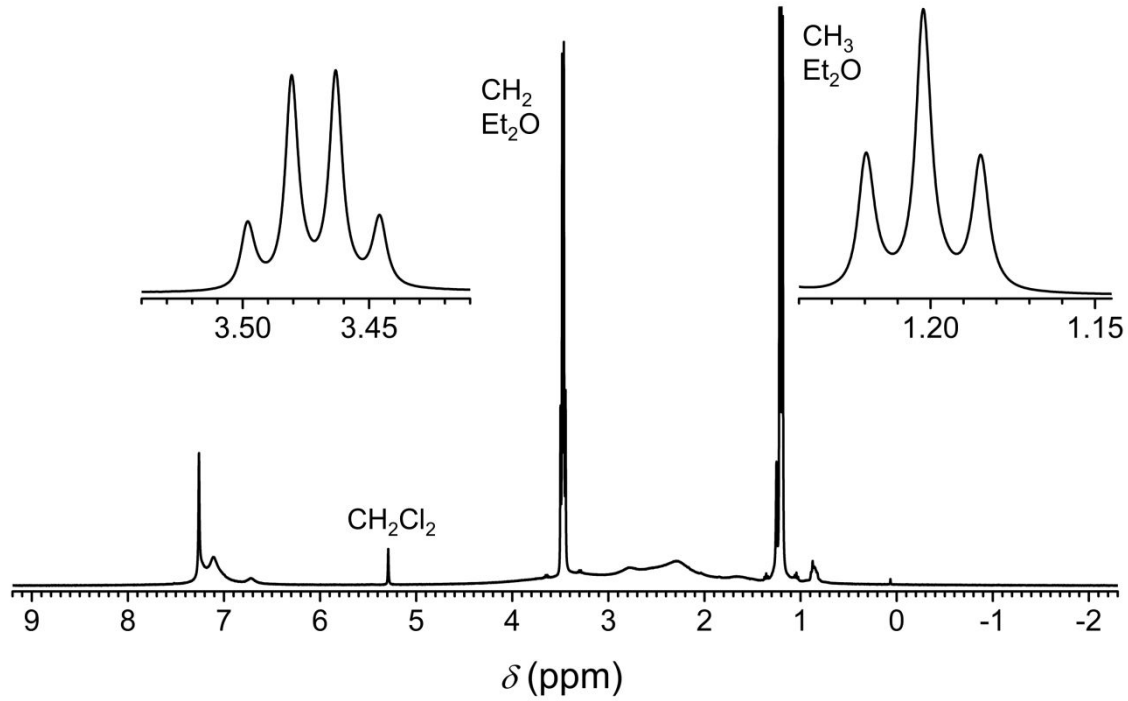


**Figure S2.** $^{1}$H-NMR spectrum of **1*h*** in $CDCl_3$ (400.13 MHz, 298 K). The narrow peaks are from $CH_2Cl_2$ (5.29 ppm), $Et_2O$ (3.47 and 1.20 ppm), and residual proton impurities in the solvent (7.26 ppm). The $CH_2$ signals of $Et_2O$ and $CH_2Cl_2$ have a 4.00:0.13 area ratio, indicating a $Et_2O/CH_2Cl_2$ molar ratio of 15, in good agreement with the value obtained from elemental analysis (14.6). Processing parameters (TopSpin 4.3.0[1]): SI = TD, LB = 0.30 Hz.

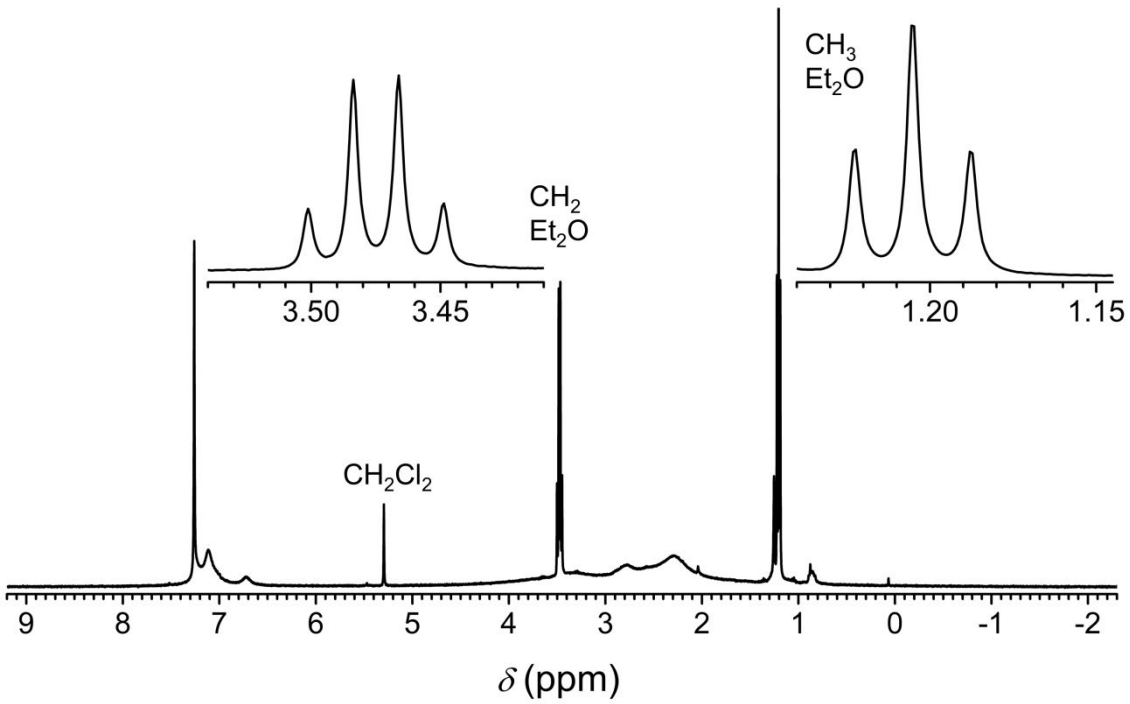


**Figure S3.** $^{1}$H-NMR spectrum of **1*m*** in $CDCl_3$ (400.13 MHz, 298 K). The narrow peaks are from $CH_2Cl_2$ (5.30 ppm), $Et_2O$ (3.47 and 1.21 ppm), and residual proton impurities in the solvent (7.26 ppm). The $CH_2$ signals of $Et_2O$ and $CH_2Cl_2$ have a 4.00:0.52 area ratio, indicating a $Et_2O/CH_2Cl_2$ molar ratio of 3.8, in good agreement with the value obtained from elemental analysis (4.0). Processing parameters (TopSpin 4.3.0[1]): SI = TD, LB = 0.30 Hz.

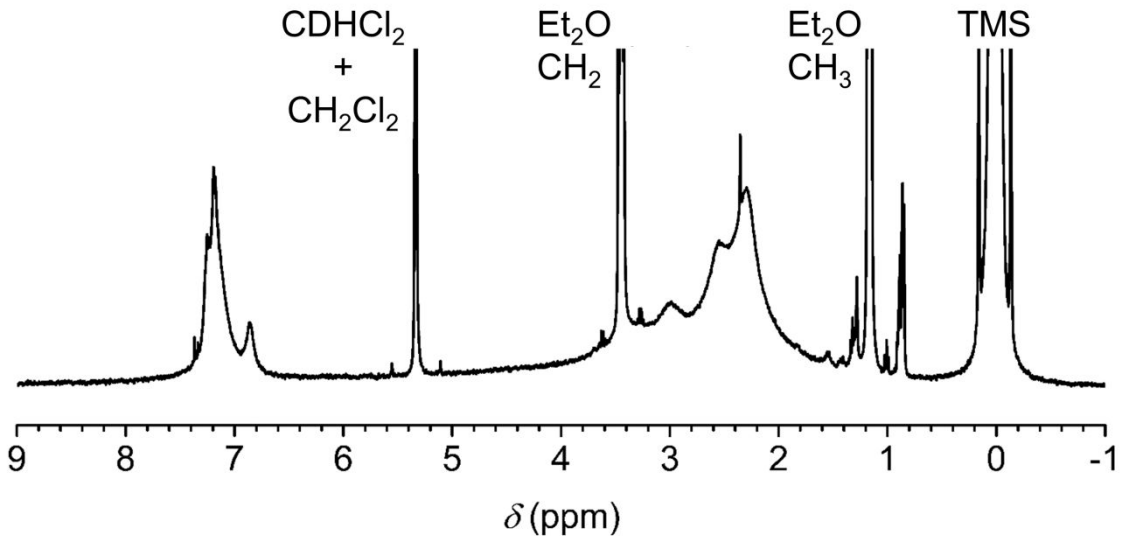


**Figure S4.** $^{1}$H-NMR spectrum of **1*h*** in $CD_2Cl_2$ (400.13 MHz, 298 K). The narrow peaks are from $CH_2Cl_2$ (5.33 ppm), $Et_2O$ (3.43 and 1.15 ppm), pump oil (1.28 and 0.88 ppm), residual proton impurities in the solvent (5.32 ppm), and TMS (0.00 ppm) which was added as an internal reference for the normalization of diffusion coefficients, following the procedure described by Stalke *et al*.[2] Processing parameters (TopSpin 4.3.0[1]): SI = TD, LB = 1.00 Hz.

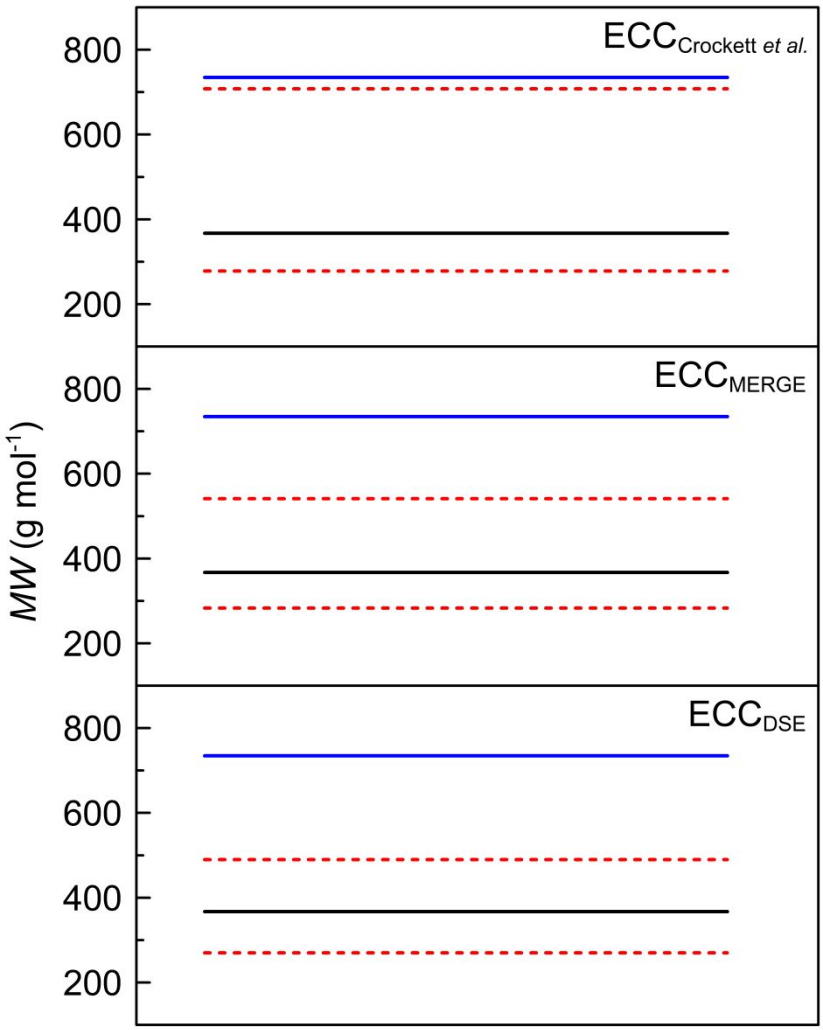


**Figure S5.** Graphical representation of estimated and calculated *MW*s. The dashed red lines represent the upper and lower limits of estimated *MW*s using each ECC. $ECC_{DSE}$ and $ECC_{MERGE}$ are from Ref.[2] while $ECC_{Crockett\ et\ al.}$ is the external calibration curve reported in Ref.[3]. The black and blue lines represent the calculated *MW*s of monomeric [VO(bdhb)] (**1'**) and dimeric **1**, respectively.

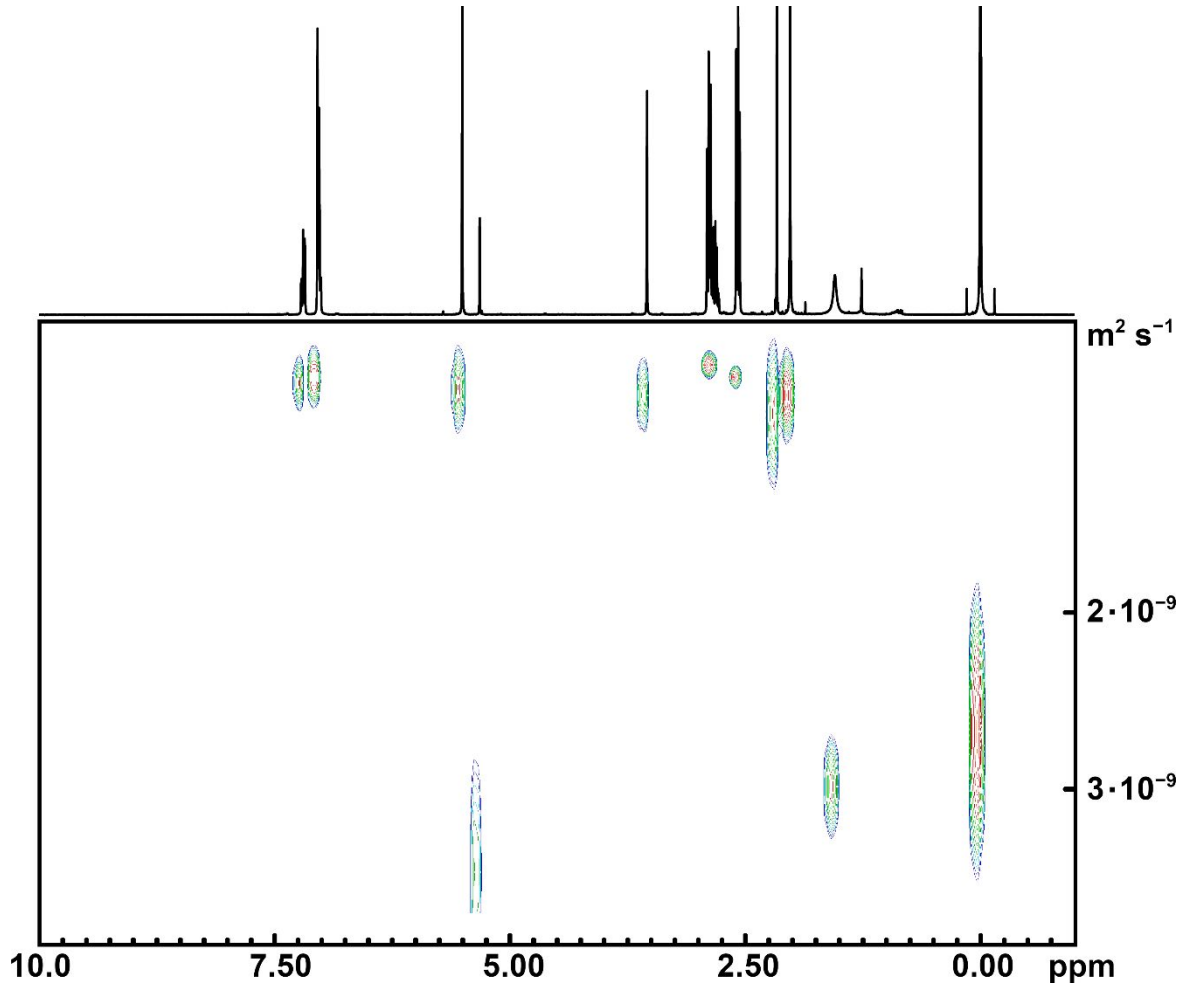


**Figure S6.** $^{1}$H-DOSY spectrum of $H_2$bdhb in $CD_2Cl_2$ (400.13 MHz, 298 K). Impurity peaks are from $H_2O$ (1.55 ppm), pump oil (1.26 and 0.89 ppm), and proton residuals in the solvent (5.32 ppm). TMS (0.00 ppm) was added as an internal reference for the normalization of diffusion coefficients, following the procedure described by Stalke *et al*.[2] Processing parameters (TopSpin 4.3.0[1]): SI = TD, LB = 0.30 Hz.

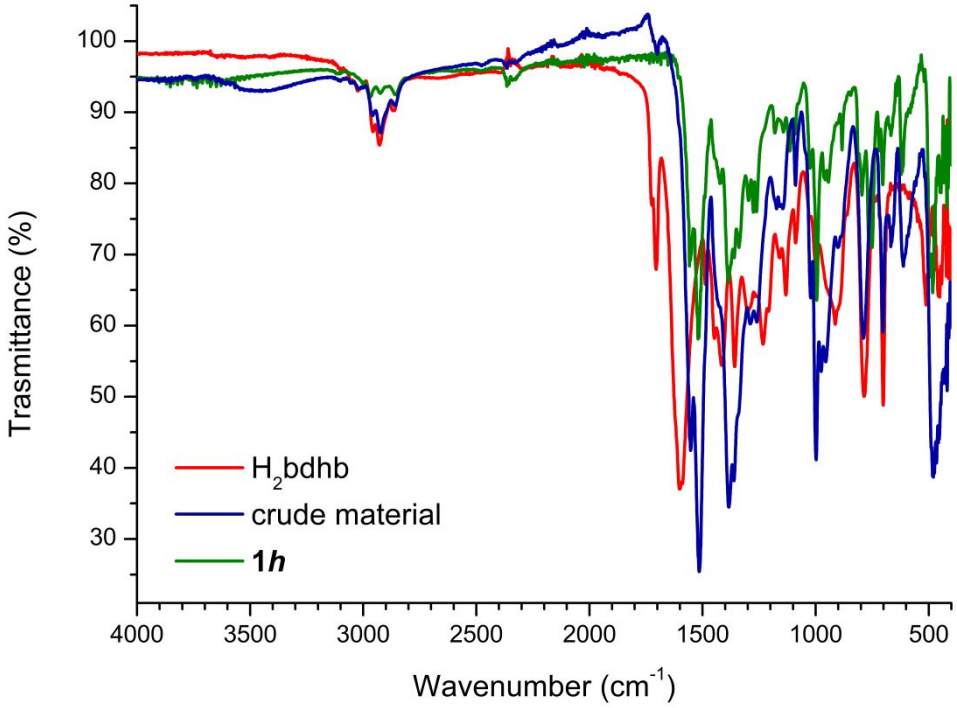


**Figure S7.** FT-IR spectra of $H_2$bdhb (red), the crude material (blue), and crystalline **1*h*** (green).

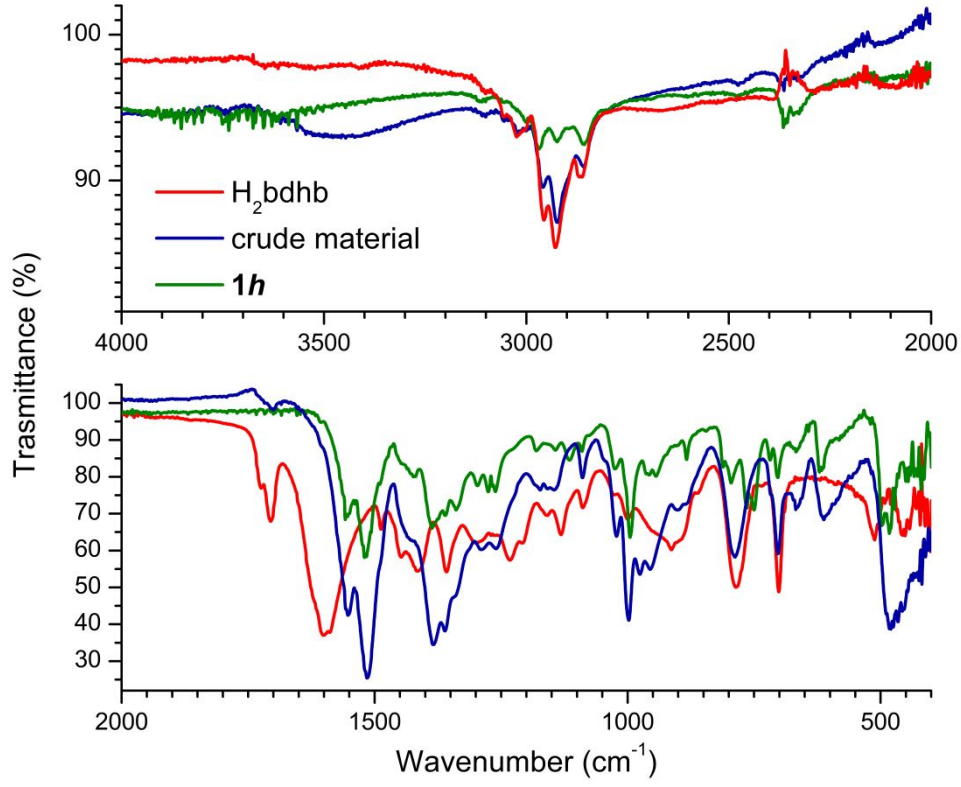


**Figure S8.** FT-IR spectra of $H_2$bdhb (red), the crude material (blue), and crystalline **1*h*** (green) in the region 4000–2000 $cm^{-1}$ (top) and 2000–400 $cm^{-1}$ (bottom). The presence of $H_2O$ and EtOH molecules is reflected by the broad O-H stretching signal observed around 3450 $cm^{-1}$. The intense bands of the proligand between 1724 and 1602 $cm^{-1}$, which contain contributions from C=O and C=C stretching, are red shifted by approximately 100 $cm^{-1}$ upon coordination.

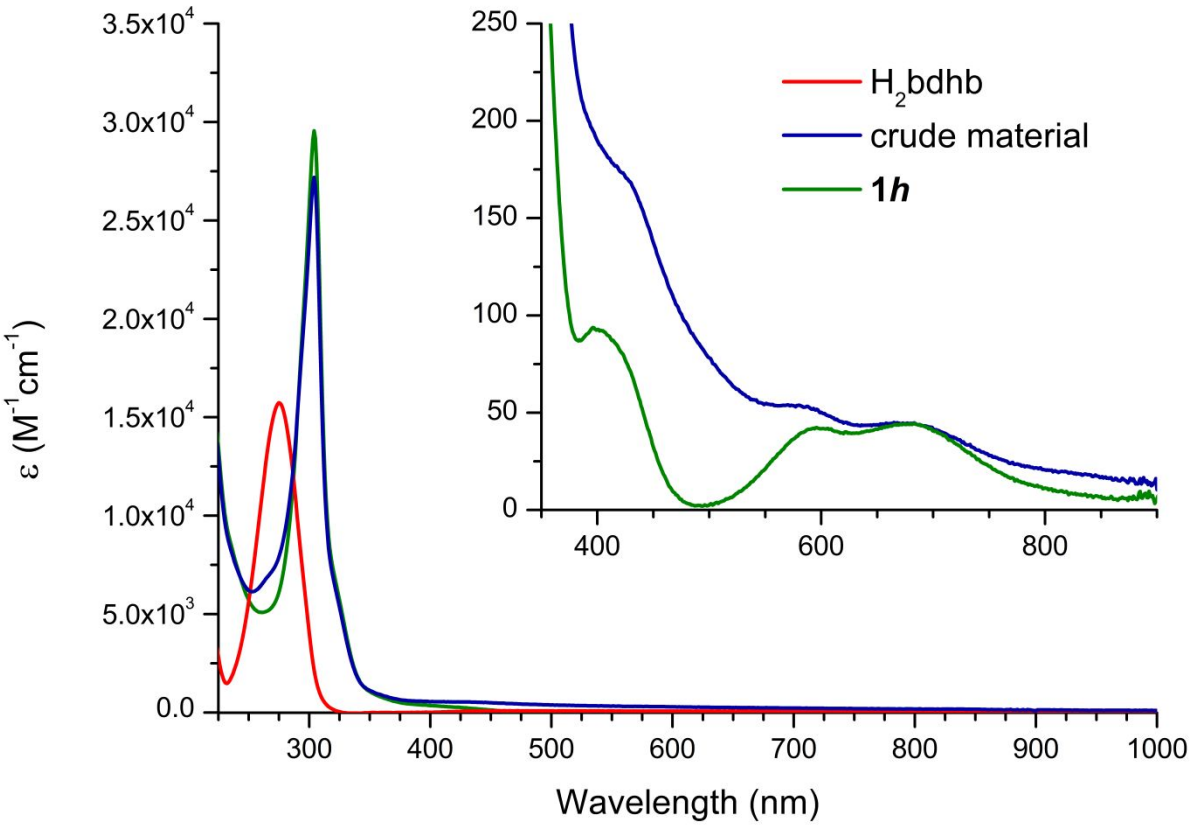


**Figure S9.** UV-Vis-NIR spectra of $H_2$bdhb (red), the crude material (blue), and crystalline **1*h*** (green) in $CH_2Cl_2$. The inset shows the characteristic absorption bands of vanadyl complexes.

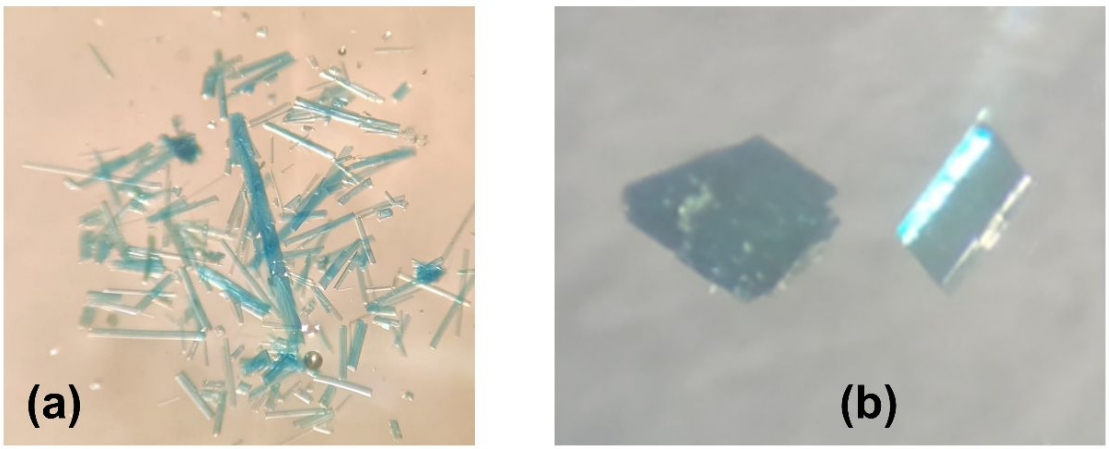


**Figure S10.** (a) Rod-like trigonal crystals of **1*h*** and (b) parallelogram-shaped crystals of monoclinic solvatomorph **1*m***.

**Table S1.** Crystal data and refinement parameters for **1*h***, **1*m***, and **1*a***.

| | | | |
|---|---|---|---|
| Chemical formula | $C_{43.73}H_{59.26}Cl_{0.26}O_{11.90}V_2$ (**1*h***) [a] | $C_{39.69}H_{49.16}Cl_{0.21}O_{10.90}V_2$ (**1*m***) [b] | $C_{36}H_{40}O_{10}V_2$ (**1*a***) |
| Formula weight | 886.42 | 809.81 | 734.56 |
| $T$ (K) | 100(2) | 100(2) | 100(2) |
| Crystal size ($mm^3$) | 0.900 × 0.172 × 0.172 | 0.120 × 0.060 × 0.040 | 0.250 × 0.150 × 0.050 |
| Radiation | Cu-Kα (λ = 1.54178 Å) | Cu-Kα (λ = 1.54178 Å) | Cu-Kα (λ = 1.54178 Å) |
| Crystal system | trigonal | monoclinic | triclinic |
| Space group | $R\bar{3}$ | $P2_1/c$ | $P\bar{1}$ |
| $a$ (Å) | 44.7168(10) | 7.4835(2) | 7.4876(4) |
| $b$ (Å) | 44.7168(10) | 11.9824(3) | 8.5547(5) |
| $c$ (Å) | 7.4408(3) | 21.7146(5) | 13.6688(8) |
| $\alpha$ (deg) | 90 | 90 | 101.870(3) |
| $\beta$ (deg) | 90 | 96.492(2) | 93.469(3) |
| $\gamma$ (deg) | 120 | 90 | 97.046(3) |
| $V$ ($Å^3$) | 12885.2(8) | 1934.67(8) | 847.03(8) |
| $Z$ | 9 | 2 | 1 |
| $\rho_{calcd}$ (g $cm^{-3}$) | 1.028 | 1.390 | 1.440 |
| $\vartheta_{min}/\vartheta_{max}$ (deg) | 3.424/72.372 | 4.098/68.373 | 3.317/68.471 |
| Refls. collect./indep. | 57672/5668 | 40710/3538 | 21316/3093 |
| $R_{int}$ | 0.0540 | 0.0992 | 0.0598 |
| Parameters/restraints | 219/0 | 272/31 | 220/0 |
| $R1/wR2$ (all data) | 0.0330/0.0979 | 0.0498/0.0944 | 0.0533/0.1426 |
| $R1/wR2$ ($I \geq 2\sigma(I)$) | 0.0311/0.0966 | 0.0397/0.0898 | 0.0494/0.1384 |
| GOF | 1.098 | 1.064 | 1.124 |
| $\Delta F$ max/min ($e$Å$^{-3}$) | 0.348/–0.338 | 0.323/–0.343 | 0.415/–0.776 |

[a]The given chemical formula and other crystal data include the solvent molecules in the channels, whose contribution to the scattering of X-rays was removed using the SQUEEZE routine.[4] [b]The given chemical formula corresponds to **1**·0.895$Et_2O$·0.105$CH_2Cl_2$ and results from structure refinement; $^1$H-NMR and elemental analysis on the bulk material gave **1**·0.80$Et_2O$·0.20$CH_2Cl_2$.

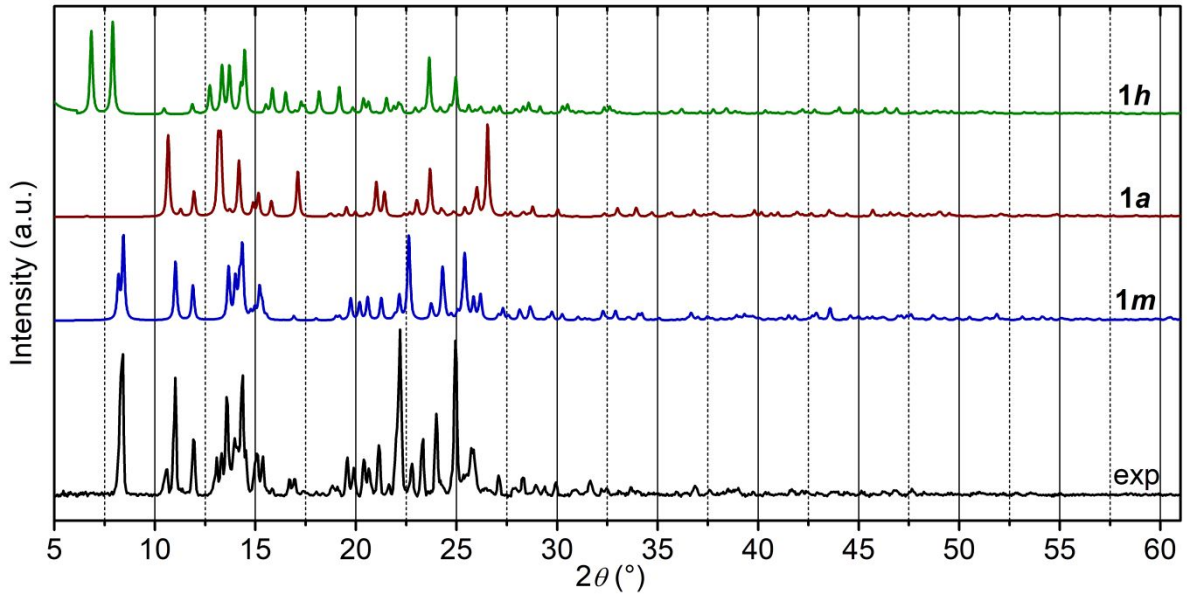


**Figure S11.** Background-subtracted PXRD pattern of the crystalline solid obtained upon transformation of **1*h*** (black), recorded at room temperature and with Cu-Kα radiation. The figure also shows the PXRD patterns of **1*m***, **1*a***, and **1*h*** simulated from their X-ray structures at 100 K using Mercury 2021.1.0,[5] with a full-width-at-half-maximum of 0.15° in 2$\theta$.

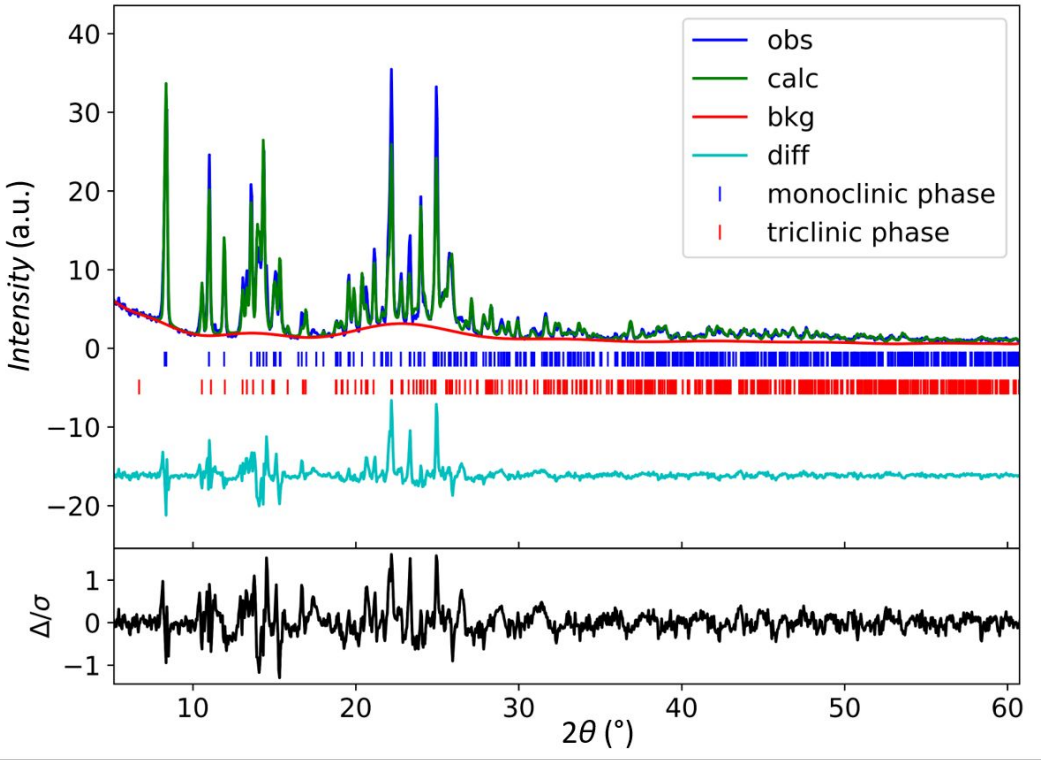


**Figure S12.** The Rietveld observed (blue line), calculated (green line) and difference curve (cyan line) of the refined pattern of the crystalline solid obtained upon transformation of **1*h***. The black curve at the bottom represents the weighted difference between the observed and calculated diffraction patterns. The ticks indicate the calculated positions of the reflections for the monoclinic (**1*m***) and triclinic (**1*a***) phases, with the color code indicated in the legend.

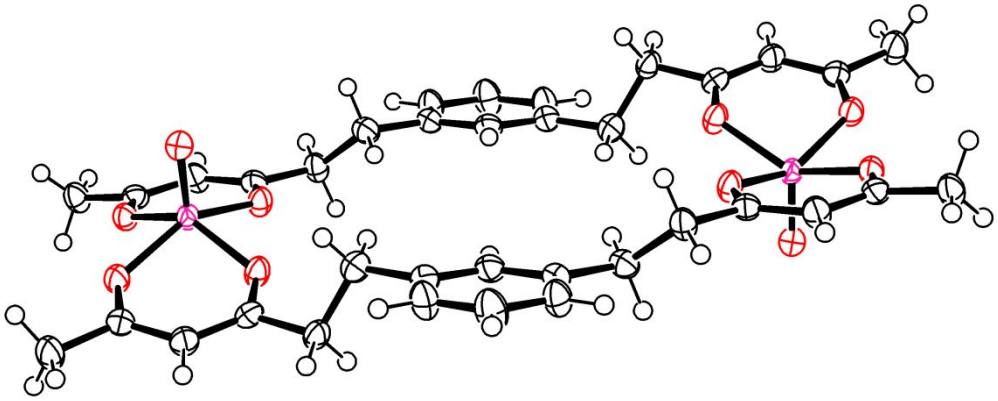

**Figure S13.** ORTEP-3[6] plot of the divanadium(IV) complex in **1*h***. Displacement ellipsoids are drawn at the 60% probability level while H atoms are depicted as spheres of arbitrary radius. Color code: pink (V), red (O), black (C and H).

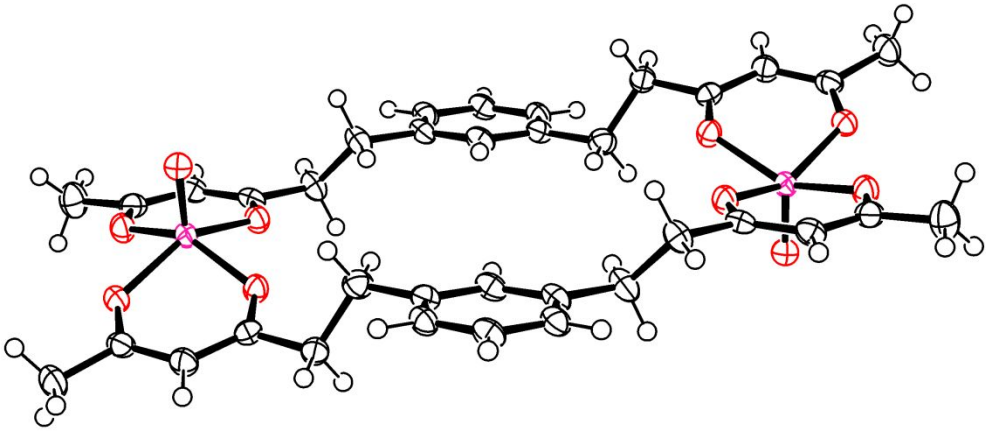

**Figure S14.** ORTEP-3[6] plot of the divanadium(IV) complex in **1*m***. Displacement ellipsoids are drawn at the 60% probability level while H atoms are depicted as spheres of arbitrary radius. The color code is the same as in Figure S13.

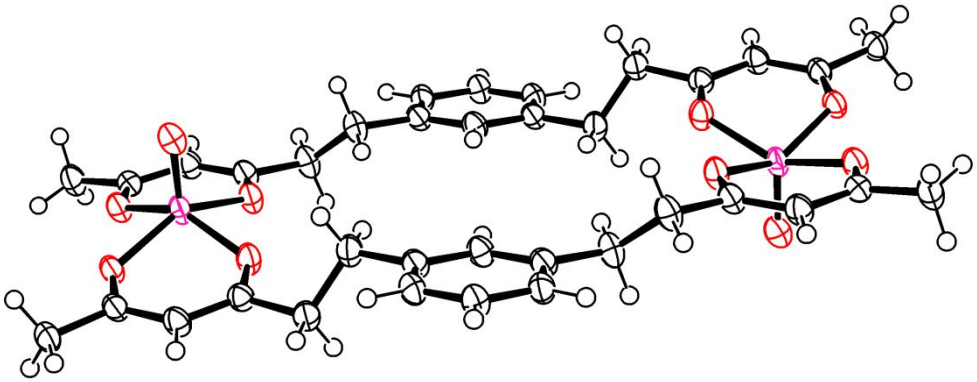

**Figure S15.** ORTEP-3[6] plot of the divanadium(IV) complex in **1*a***, omitting rotational disorder of $CH_3$ groups. Displacement ellipsoids are drawn at the 60% probability level while H atoms are depicted as spheres of arbitrary radius. The color code is the same as in Figure S13.

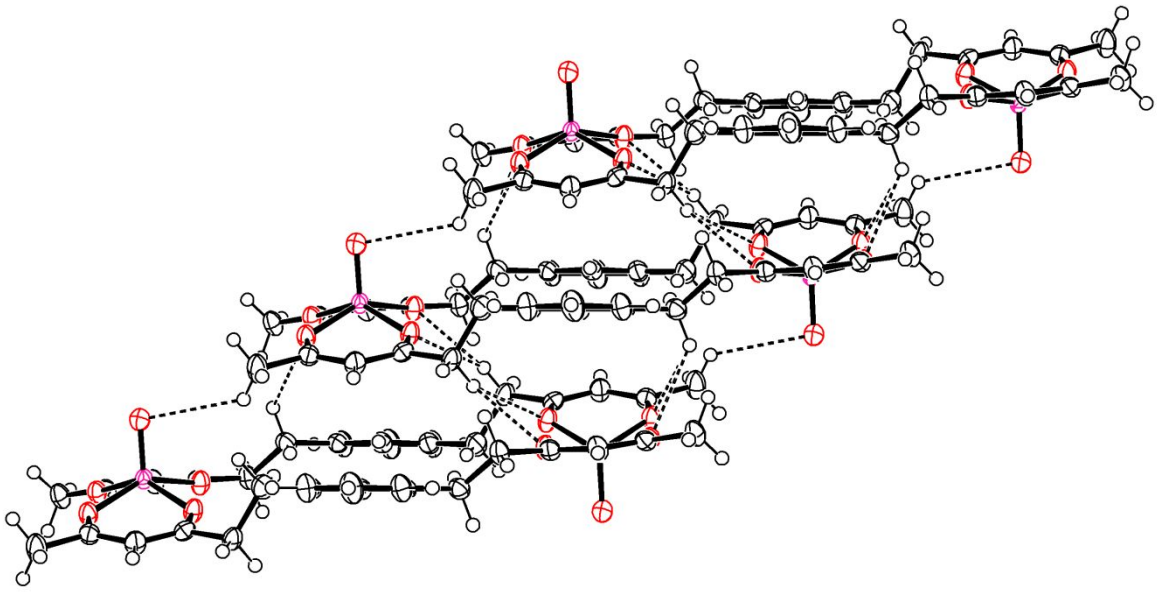

**Figure S16.** ORTEP-3[6] side view of divanadium(IV) complexes stacked into columns in **1*h***, with potential C–H···O hydrogen bonds depicted as dashed lines. Molecules are related by unitary translations along *z*. Displacement ellipsoids are drawn at the 60% probability level while H atoms are depicted as spheres of arbitrary radius. The color code is the same as in Figure S13.

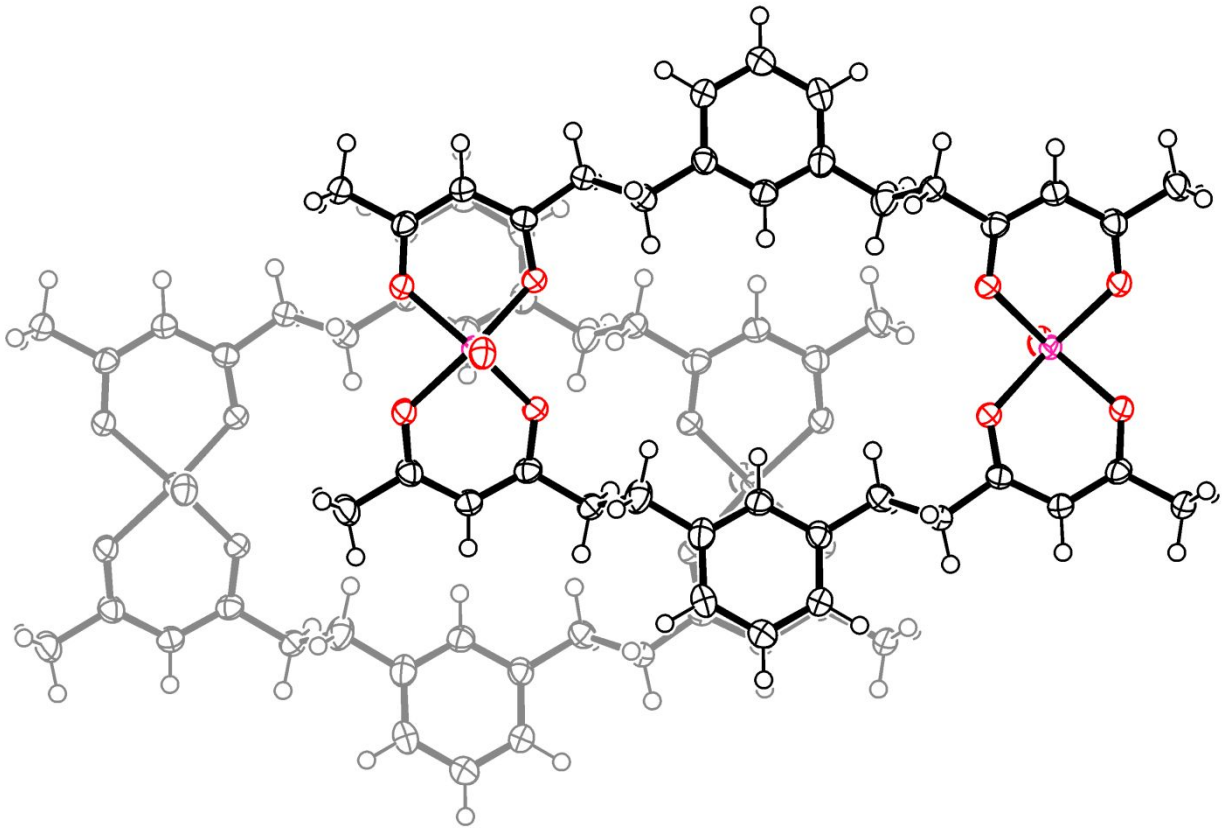

**Figure S17.** ORTEP-3[6] top view of two stacked divanadium(IV) complexes in **1*h***. Displacement ellipsoids are drawn at the 60% probability level while H atoms are depicted as spheres of arbitrary radius. The color code for the top molecule is the same as in Figure S13. The bottom molecule is translated by –1 along *z* and is depicted in grey.

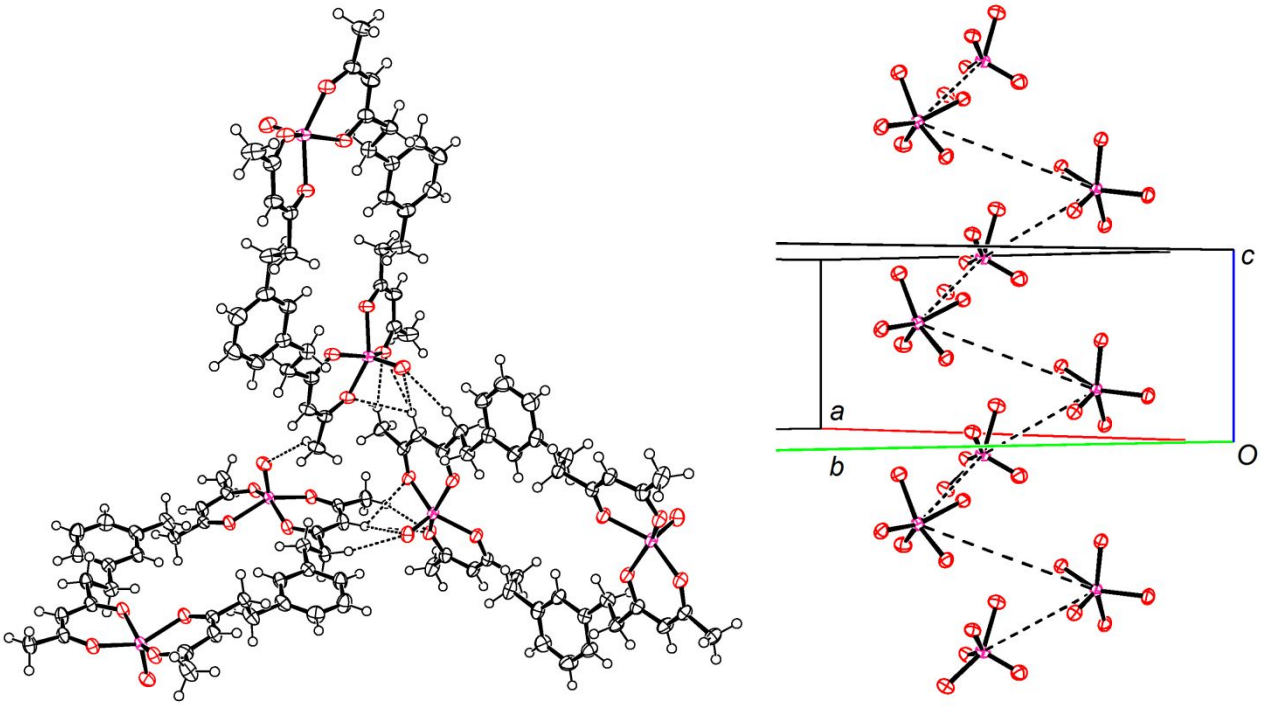


**Figure S18.** (Left) ORTEP-3[6] plot of three divanadium(IV) complexes related by a $3_1$ axis in **1*h***, as viewed along *z* and with potential C–H···O hydrogen bonds depicted as dashed lines. (Right) The 1D helical chain of intermolecular dipolar interactions between metal centers spiralizing along a $3_1$ axis in **1*h***, as viewed approximately orthogonal to *z* and including only the donor O atoms. The dashed lines highlight the shortest V···V distances in the crystal [7.1488(4) Å]. Displacement ellipsoids are drawn at the 60% probability level while H atoms are depicted as spheres of arbitrary radius. The color code is the same as in Figure S13.

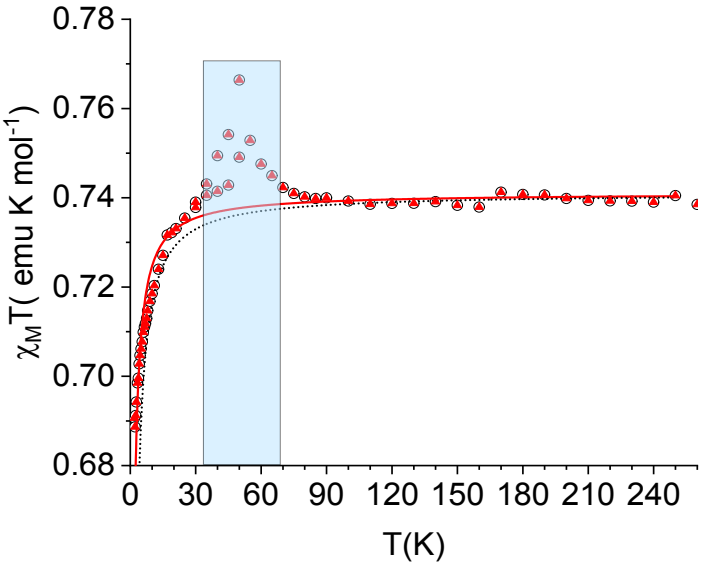


**Figure S19.** $\chi_M T$ vs. $T$ curve recorded with an applied dc field of 1 kOe up to 30 K and of 10 kOe above 30 K on a microcrystalline sample of **1*h***, and best-fit curves obtained by using Eggert-Affleck-Takahashi equation for an antiferromagnetic regular spin-chain (red solid line) or Bleaney-Bowers equation for a dimer (black dashed line); see main text for more details. The feature at ca. 50 K is due to the onset of the antiferromagnetic transition of residual dioxygen present in the sample chamber. The data in the shaded area were not included in the fitting procedure.

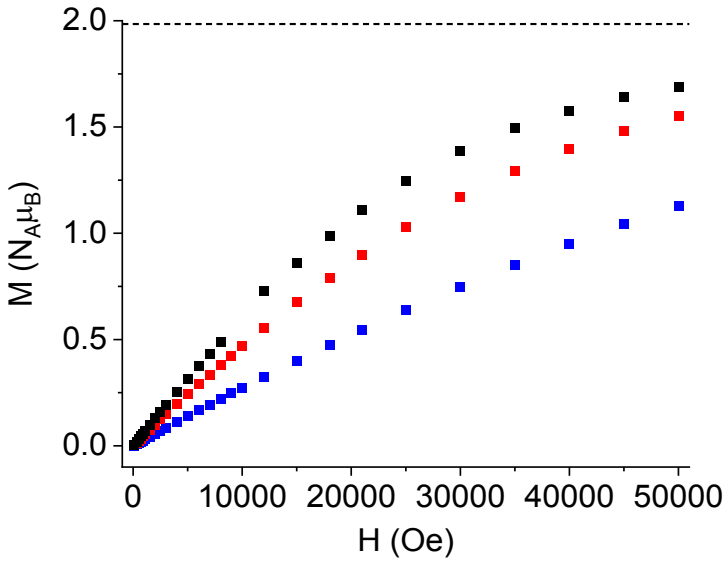


**Figure S20.** Field-dependent isothermal magnetization curves recorded at 1.9 K (black), 2.4 K (red), and 4.5 K (blue) on a microcrystalline sample of **1*h***. The horizontal dashed line is the saturation value expected for two uncorrelated $S$ = 1/2 spins with $g$ = 1.988.

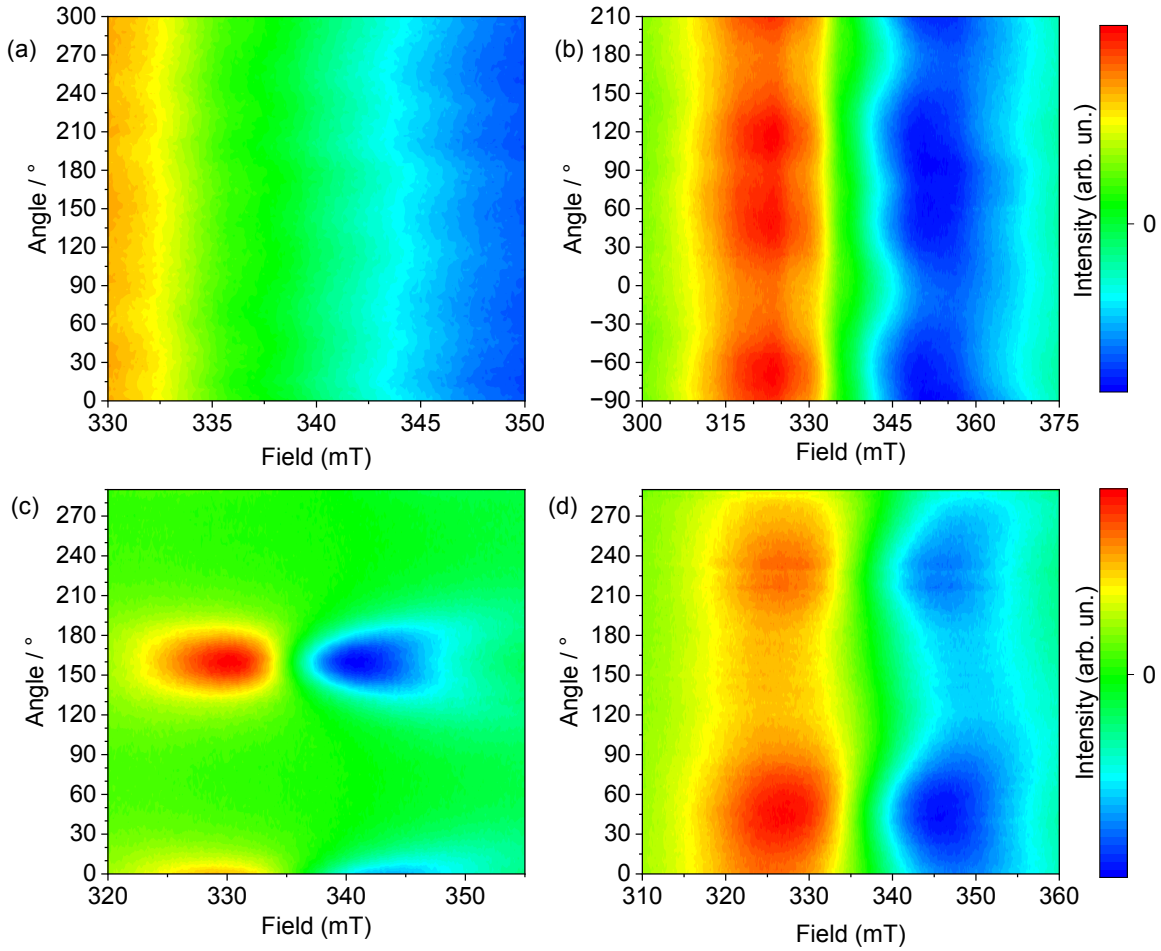


**Figure S21.** Upper panels: angle-dependent EPR spectra of **1*h*** at 50 K as the magnetic field is rotated in the *ab* plane (a) and from the *c* axis (angle = 0°) to the *ab* plane (b). Lower panels: angle-dependent EPR spectra of **1*m*** at 50 K as the magnetic field is rotated in the *ac* plane (c) and in a plane containing the *b* axis (d).

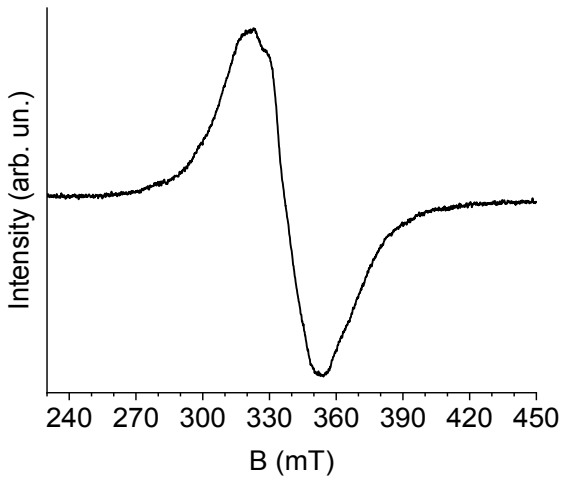


**Figure S22.** X-band CW-EPR spectrum of a single crystal of **1*h***, measured at 50 K with the magnetic field along the *c* axis.

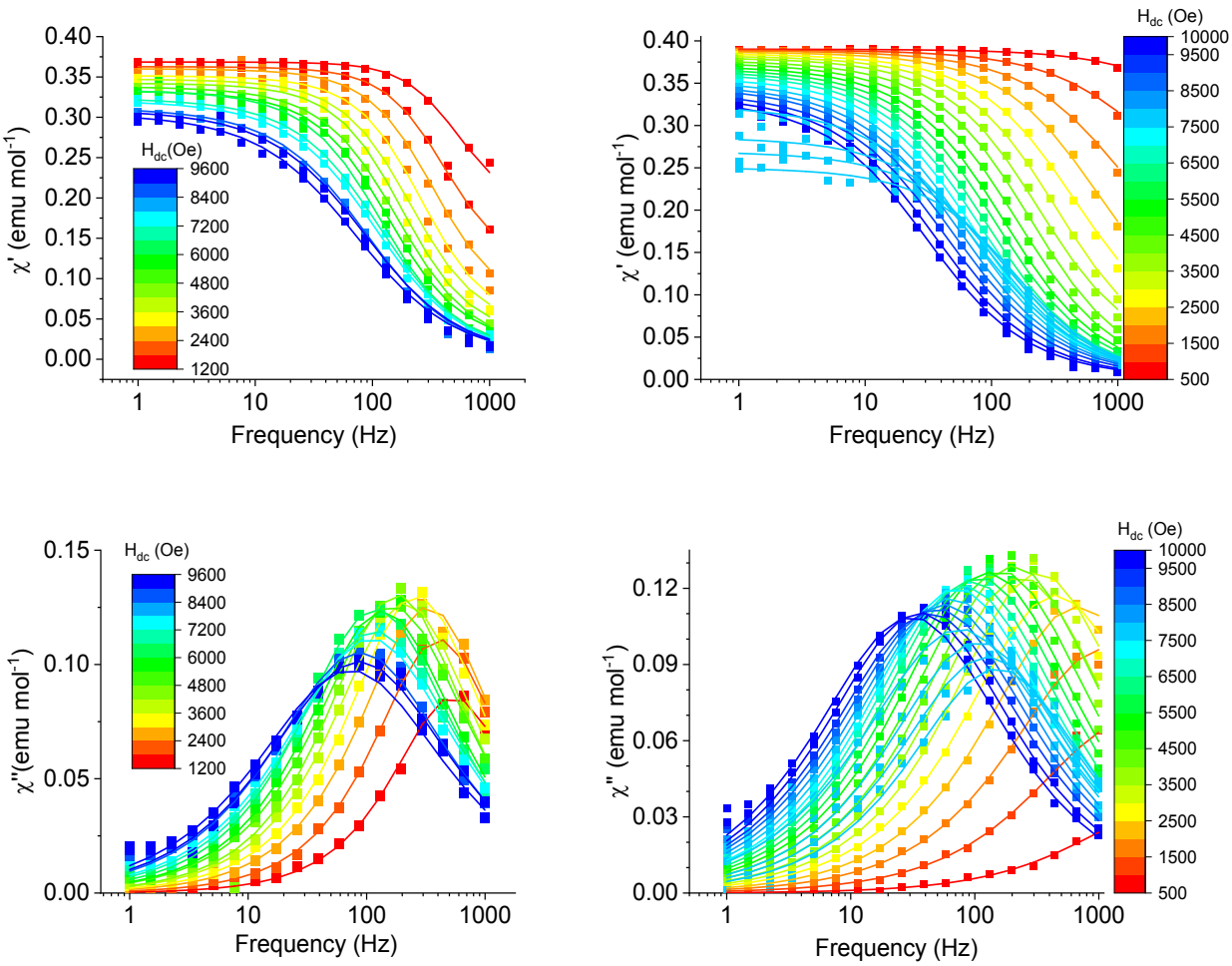


**Figure S23.** Variable-frequency ac susceptibility of **1*h*** (left) and **1*m*** (right) as a function of applied dc field, measured at 1.9 K. The solid lines represent the best-fit curves obtained using a generalized Debye model and the parameters reported in Tables S2 and S3.

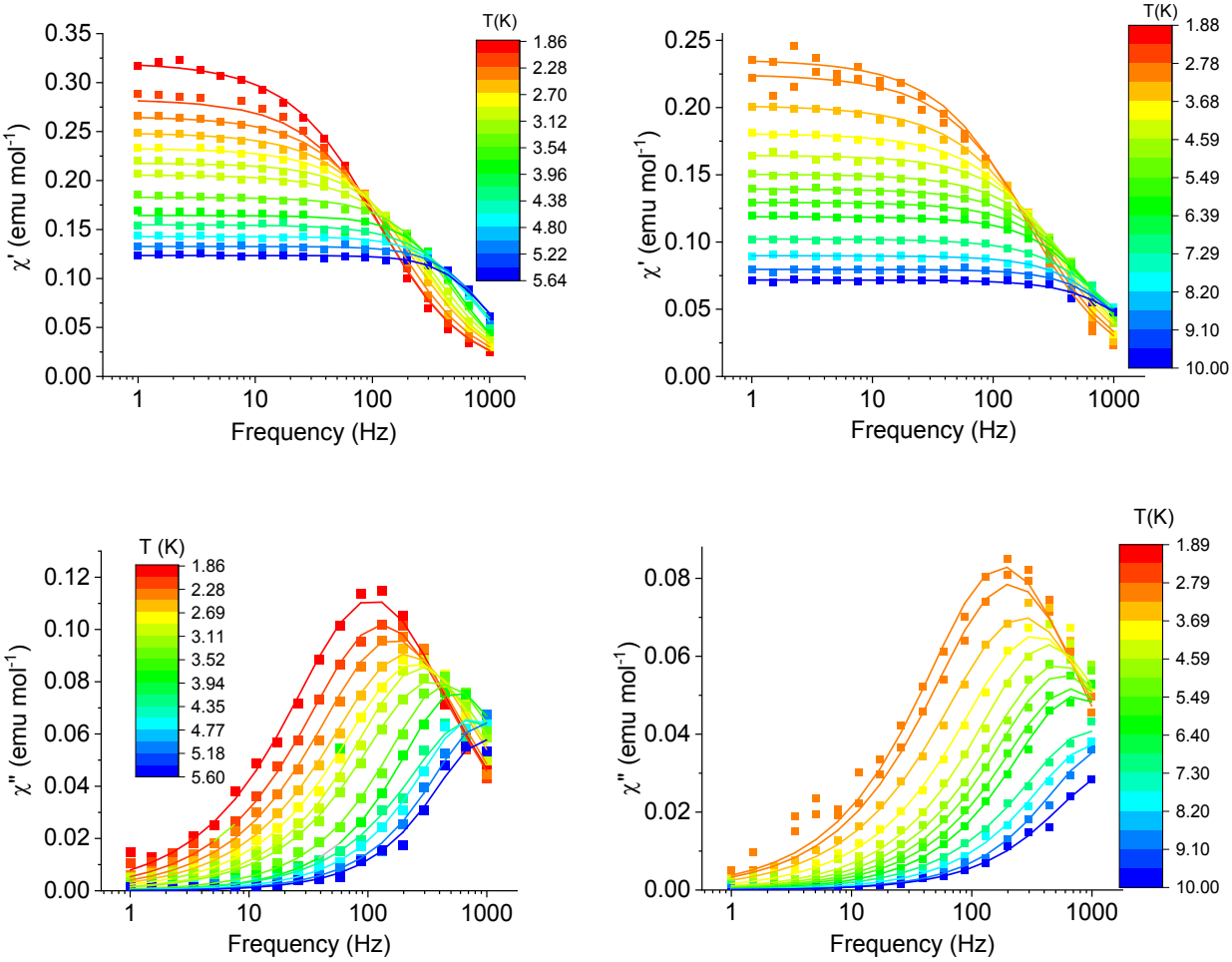


**Figure S24.** Variable-frequency ac susceptibility of **1*h*** (left) and **1*m*** (right) as a function of temperature, measured in dc fields of 7200 Oe and 7500 Oe, respectively. The solid lines are the best-fit curves obtained using a generalized Debye model and the parameters reported in Tables S2 and S3.

**Table S2.** Best-fit parameters for frequency dependent ac susceptibility curves of **1*h***.[a]

| $\chi_T-\chi_S$ (emu mol$^{-1}$) | | $\tau$ (s) | | $\alpha$ | | $\chi_S$ (emu mol$^{-1}$) | | $T$ (K) | $H_{dc}$ (Oe) |
|---|---|---|---|---|---|---|---|---|---|
| 0.1808 | 0.04914 | 2.970E-4 | 5.432E-5 | 0.03327 | 0.1514 | 0.1877 | 0.06398 | 1.892 | 1200 |
| 0.2474 | 0.02475 | 3.920E-4 | 4.838E-5 | 0.06864 | 0.04605 | 0.1154 | 0.02872 | 1.900 | 1800 |
| 0.2951 | 0.02292 | 4.850E-4 | 3.585E-5 | 0.1038 | 0.03910 | 0.06515 | 0.02827 | 1.895 | 2400 |
| 0.3090 | 0.02424 | 6.059E-4 | 4.504E-5 | 0.1077 | 0.03803 | 0.04261 | 0.03016 | 1.933 | 3000 |
| 0.3104 | 0.03039 | 7.554E-4 | 5.879E-5 | 0.1264 | 0.04060 | 0.03698 | 0.03943 | 1.899 | 3600 |
| 0.3147 | 0.05650 | 8.839E-4 | 9.398E-5 | 0.1177 | 0.07577 | 0.02772 | 0.07476 | 2.006 | 4200 |
| 0.3265 | 0.03606 | 9.750E-4 | 8.275E-5 | 0.1636 | 0.04327 | 0.01178 | 0.04588 | 1.900 | 4800 |
| 0.3159 | 0.07284 | 0.001165 | 1.083E-4 | 0.1544 | 0.08652 | 0.01710 | 0.09806 | 1.897 | 5400 |
| 0.3261 | 0.07987 | 0.001326 | 1.357E-4 | 0.1697 | 0.09056 | 0.007777 | 0.1068 | 1.894 | 6000 |
| 0.3223 | 0.07293 | 0.001367 | 1.807E-4 | 0.2125 | 0.07915 | 0.001650 | 0.09418 | 1.900 | 6600 |
| 0.3210 | 0.09123 | 0.001470 | 2.079E-4 | 0.2278 | 0.08880 | 3.726E-14 | 0.1211 | 1.897 | 7200 |
| 0.3123 | 0.08185 | 0.001810 | 2.394E-4 | 0.2438 | 0.08839 | 2.220E-14 | 0.1054 | 1.900 | 8400 |
| 0.3099 | 0.09961 | 0.001846 | 3.165E-4 | 0.2623 | 0.1036 | 2.739E-14 | 0.1270 | 1.933 | 9000 |
| 0.3053 | 0.1337 | 0.002182 | 5.120E-4 | 0.2763 | 0.1269 | 2.222E-14 | 0.1734 | 1.894 | 9600 |
| 0.2817 | 0.1633 | 0.001204 | 2.938E-4 | 0.2025 | 0.2011 | 0.001496 | 0.2154 | 2.164 | 7200 |
| 0.2625 | 0.06352 | 9.786E-4 | 9.675E-5 | 0.1936 | 0.08466 | 0.003157 | 0.08409 | 2.300 | 7200 |
| 0.2488 | 0.04207 | 7.552E-4 | 5.392E-5 | 0.1983 | 0.05920 | 3.395E-12 | 0.05540 | 2.500 | 7200 |
| 0.2331 | 0.03994 | 6.353E-4 | 7.076E-5 | 0.1822 | 0.06664 | 2.221E-14 | 0.05153 | 2.723 | 7200 |
| 0.2131 | 0.04598 | 5.637E-4 | 5.523E-5 | 0.1389 | 0.08545 | 0.004755 | 0.06154 | 2.900 | 7200 |
| 0.2059 | 0.03141 | 4.629E-4 | 3.590E-5 | 0.1558 | 0.06077 | 4.222E-13 | 0.04130 | 3.100 | 7200 |
| 0.1811 | 0.02784 | 3.459E-4 | 3.099E-5 | 0.08616 | 0.07040 | 0.001746 | 0.03673 | 3.499 | 7200 |
| 0.1643 | 0.07247 | 2.826E-4 | 9.446E-5 | 0.04642 | 0.2271 | 2.933E-14 | 0.08997 | 4.093 | 7200 |
| 0.1543 | 0.05028 | 2.171E-4 | 8.794E-5 | 0.1055 | 0.1315 | 5.686E-4 | 0.05661 | 4.299 | 7200 |
| 0.1404 | 0.02368 | 2.067E-4 | 2.893E-5 | 0.03916 | 0.08413 | 0.002372 | 0.02917 | 4.699 | 7200 |
| 0.1327 | 0.03480 | 1.658E-4 | 6.004E-5 | 0.02041 | 0.1105 | 1.182E-8 | 0.03667 | 5.099 | 7200 |
| 0.1155 | 0.04336 | 1.628E-4 | 8.246E-5 | 9.839E-13 | 0.1490 | 0.007865 | 0.04579 | 5.499 | 7200 |

[a]For each best-fit parameter ($\chi_T-\chi_S$, $\tau$, $\alpha$, $\chi_S$) the second column gives the associated uncertainty.

**Table S3.** Best-fit parameters for frequency dependent ac susceptibility curves of **1*m*.**[a]

| $\chi_T-\chi_S$ (emu mol$^{-1}$) | | $\tau$ (s) | | $\alpha$ | | $\chi_S$ (emu mol$^{-1}$) | | $T$ (K) | $H_{dc}$ (Oe) |
|---|---|---|---|---|---|---|---|---|---|
| 0.09361 | 0.1058 | 4.745E-5 | 9.248E-5 | 0.2382 | 0.2554 | 0.2965 | 0.1088 | 1.900 | 500 |
| 0.2028 | 0.05294 | 9.293E-5 | 4.223E-5 | 0.2564 | 0.07774 | 0.1867 | 0.05601 | 1.900 | 1000 |
| 0.2874 | 0.05066 | 1.479E-4 | 4.096E-5 | 0.2507 | 0.05174 | 0.1013 | 0.05418 | 1.900 | 1500 |
| 0.3300 | 0.02485 | 2.355E-4 | 2.497E-5 | 0.2362 | 0.02657 | 0.05712 | 0.02779 | 1.900 | 2000 |
| 0.3426 | 0.04368 | 3.549E-4 | 5.621E-5 | 0.2353 | 0.04734 | 0.04229 | 0.05018 | 1.900 | 2500 |
| 0.3612 | 0.03656 | 4.863E-4 | 4.926E-5 | 0.2237 | 0.03864 | 0.02142 | 0.04427 | 1.900 | 3000 |
| 0.3555 | 0.04209 | 6.798E-4 | 5.605E-5 | 0.2220 | 0.04386 | 0.02497 | 0.05416 | 1.900 | 3500 |
| 0.3773 | 0.06957 | 7.764E-4 | 1.054E-4 | 0.2368 | 0.06300 | 1.257E-13 | 0.08778 | 1.900 | 4000 |
| 0.3746 | 0.08261 | 9.925E-4 | 1.455E-4 | 0.2418 | 0.07331 | 2.235E-14 | 0.1056 | 1.900 | 4500 |
| 0.3694 | 0.09430 | 0.001256 | 2.117E-4 | 0.2357 | 0.08673 | 0.001598 | 0.1193 | 1.900 | 5000 |
| 0.3683 | 0.09228 | 0.001460 | 2.028E-4 | 0.2433 | 0.07785 | 2.312E-14 | 0.1195 | 1.900 | 5500 |
| 0.3655 | 0.1096 | 0.001719 | 2.883E-4 | 0.2451 | 0.09040 | 2.222E-14 | 0.1438 | 1.900 | 6000 |
| 0.3629 | 0.1068 | 0.001958 | 3.046E-4 | 0.2505 | 0.08976 | 2.221E-14 | 0.1400 | 1.900 | 6500 |
| 0.3577 | 0.1057 | 0.002221 | 3.825E-4 | 0.2474 | 0.09308 | 2.221E-14 | 0.1376 | 1.900 | 7000 |
| 0.3536 | 0.1131 | 0.002489 | 4.093E-4 | 0.2599 | 0.09175 | 2.221E-14 | 0.1491 | 1.900 | 7500 |
| 0.3496 | 0.08819 | 0.002828 | 3.847E-4 | 0.2655 | 0.07671 | 2.221E-14 | 0.1149 | 1.900 | 8000 |
| 0.3470 | 0.09692 | 0.003234 | 4.859E-4 | 0.2699 | 0.08225 | 2.352E-14 | 0.1266 | 1.900 | 8500 |
| 0.3408 | 0.09290 | 0.003714 | 4.777E-4 | 0.2681 | 0.07529 | 2.221E-14 | 0.1234 | 1.900 | 9000 |
| 0.3363 | 0.06633 | 0.004427 | 4.765E-4 | 0.2602 | 0.06043 | 2.222E-14 | 0.08641 | 1.900 | 9500 |

| | | | | | | | | | |
|---|---|---|---|---|---|---|---|---|---|
| 0.3326 | 0.06133 | 0.005193 | 5.884E-4 | 0.2622 | 0.05862 | 2.221E-14 | 0.07886 | 1.900 | 10000 |
| 0.3248 | 0.1274 | 0.002104 | 4.312E-4 | 0.2747 | 0.1164 | 2.354E-14 | 0.1651 | 2.100 | 7500 |
| 0.2862 | 0.08409 | 0.001501 | 1.956E-4 | 0.2297 | 0.09860 | 2.221E-14 | 0.1079 | 2.300 | 7500 |
| 0.2694 | 0.1106 | 0.001255 | 2.221E-4 | 0.2297 | 0.1254 | 3.053E-13 | 0.1483 | 2.500 | 7500 |
| 0.2505 | 0.1432 | 0.001050 | 2.346E-4 | 0.2168 | 0.1642 | 2.221E-14 | 0.1976 | 2.700 | 7500 |
| 0.2359 | 0.1059 | 8.718E-4 | 1.539E-4 | 0.2197 | 0.1295 | 2.221E-14 | 0.1458 | 2.900 | 7500 |
| 0.2250 | 0.06971 | 7.585E-4 | 1.008E-4 | 0.2241 | 0.09325 | 5.779E-14 | 0.09418 | 3.100 | 7500 |
| 0.2018 | 0.04489 | 5.989E-4 | 1.137E-4 | 0.2278 | 0.08128 | 2.221E-14 | 0.05554 | 3.499 | 7500 |
| 0.1809 | 0.02656 | 4.625E-4 | 5.797E-5 | 0.2034 | 0.05670 | 2.221E-14 | 0.03318 | 3.900 | 7500 |
| 0.1645 | 0.03230 | 3.664E-4 | 4.603E-5 | 0.1685 | 0.07553 | 2.228E-14 | 0.04296 | 4.299 | 7500 |
| 0.1505 | 0.02166 | 3.035E-4 | 3.931E-5 | 0.1647 | 0.06818 | 2.221E-14 | 0.02637 | 4.699 | 7500 |
| 0.1395 | 0.02185 | 2.738E-4 | 5.596E-5 | 0.1453 | 0.06865 | 2.241E-14 | 0.02463 | 5.099 | 7500 |
| 0.1295 | 0.01416 | 2.357E-4 | 3.120E-5 | 0.1434 | 0.05009 | 2.312E-14 | 0.01630 | 5.499 | 7500 |
| 0.1188 | 0.01493 | 2.154E-4 | 3.807E-5 | 0.1121 | 0.05255 | 5.329E-10 | 0.01651 | 5.999 | 7500 |
| 0.1023 | 0.01852 | 1.611E-4 | 3.799E-5 | 0.1430 | 0.07830 | 2.220E-14 | 0.02063 | 6.999 | 7500 |

[a]For each best-fit parameter ($\chi_T$—$\chi_S$, $\tau$, $\alpha$, $\chi_S$), the second column gives the associated uncertainty.

**Supplementary Note 1: EPR experiments on [VO(acac)$_2$].** The $\tau_r$ value for [VO(acac)$_2$] was derived by measuring a 3 mM solution of [VO(acac)$_2$] in toluene-$d_8$/$CD_2Cl_2$ (1:1 *v*/*v*) under the same experimental conditions used for **1*m*** (see Figure 6), yielding $\tau_r = 2.26\times10^{-11}$ s and a hydrodynamic radius of 0.36 nm. Simulation analysis of the spectra estimated for $\tau_r$ a lower limit of $1.90\times10^{-11}$ s and an upper limit of $2.66\times10^{-11}$ s, which in turn correspond to a hydrodynamic radius of 0.34 and 0.38 nm, respectively.

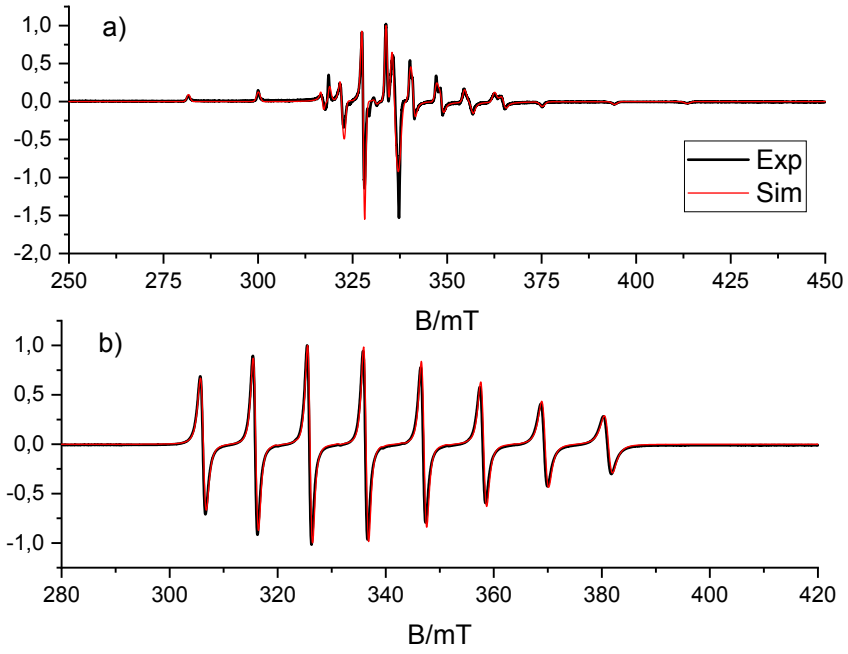


**Figure S25.** Experimental (black) and simulated (red) X-band CW-EPR spectra of [VO(acac)$_2$] recorded at 77 K (a) and RT (b) in toluene-$d_8$/$CD_2Cl_2$ (1:1 *v*/*v*).

**Table S4.** $T_1$ and $T_m$ fitting parameters.

| $T$ (K) | $T_1$ | | | | $T_m$ | | | |
|---|---|---|---|---|---|---|---|---|
| | t_fast (μs) | a_fast | t_slow (μs) | a_slow | t_fast (ns) | a_fast | t_slow (ns) | a_slow |
| 10 | 2264 | 1004 | 13680 | 1184 | 2446 | 5844 | 13416 | 7517 |
| 15 | 878 | 3816 | 4602 | 4406 | 2343 | 8251 | 11792 | 14212 |
| 20 | 375 | 1306 | 2049 | 1780 | 1948 | 5367 | 9435 | 11918 |
| 30 | 125 | 2850 | 570 | 5185 | 161 | 122809 | 6512 | 20755 |
| 50 | 39 | 10217 | 121 | 15858 | 148 | 11306 | 5787 | 28242 |
| 70 | 15 | 27662 | 37 | 48838 | - | - | 4266 | 178133 |
| 90 | 4.5 | 210568 | 13.7 | 981586 | - | - | 2958 | 354545 |

**Table S5.** Best-fit parameters in equation (5).

| $A_{dir}$ (Hz) | $A_{loc}$ (kHz) | $\hbar\omega_{loc}$ (cm$^{-1}$) |
|---|---|---|
| 4.0 | 101 | 83.7 |

**Table S6.** Differences in enthalpy and Gibbs free energy between *syn* and *anti* conformers of **1'**, along with their partition functions, computed at $T$ = 298.15 K and $p$ = 1.00 atm, in the gas phase and in different solvents, *viz.* pure toluene, pure $CH_2Cl_2$ and a mixture of toluene and $CH_2Cl_2$ (1:1 *v/v*).

| phase | $\Delta H$ (kJ mol$^{-1}$) | $\Delta G$ (kJ mol$^{-1}$) | $q$(*syn*) | $q$(*anti*) |
|---|---|---|---|---|
| gas | 3.1 | 4.9 | 0.122 | 0.878 |
| toluene | 2.9 | 4.6 | 0.133 | 0.867 |
| $CH_2Cl_2$ | 0.8 | 2.9 | 0.238 | 0.762 |
| mixture | 1.4 | 3.0 | 0.230 | 0.770 |

**Table S7.** Eigenvalues of the **g** and **A** tensors (in MHz) computed for the two conformers of **1'** in the gas phase and in different solvents, *viz.* pure toluene, pure $CH_2Cl_2$ and a mixture of toluene and $CH_2Cl_2$ (1:1 *v/v*), using two different functionals. The average values are also depicted in Italics.

| functional | phase | conformer | $g(\mathrm{tot})_x$ | $g(\mathrm{tot})_y$ | $g(\mathrm{tot})_z$ | $A_x$ | $A_y$ | $A_z$ |
|---|---|---|---|---|---|---|---|---|
| BP86 | gas | *syn* | 1.99087 | 1.98815 | 1.96758 | -133.7 | -153.1 | -438.1 |
| | | *anti* | 1.99091 | 1.98791 | 1.96750 | -128.5 | -151.9 | -433.8 |
| | | *average* | *1.99090* | *1.98794* | *1.96751* | *-129.2* | *-152.0* | *-434.3* |
| | toluene | *syn* | 1.99064 | 1.98752 | 1.96877 | -125.5 | -147.3 | -430.8 |
| | | *anti* | 1.99066 | 1.98728 | 1.96852 | -121.1 | -146.4 | -427.3 |
| | | *average* | *1.99066* | *1.98731* | *1.96855* | *-121.7* | *-146.5* | *-427.7* |
| | $CH_2Cl_2$ | *syn* | 1.99025 | 1.98637 | 1.97037 | -113.1 | -139.8 | -420.2 |
| | | *anti* | 1.99023 | 1.98613 | 1.97003 | -109.2 | -138.3 | -416.7 |
| | | *average* | *1.99024* | *1.98619* | *1.97011* | *-110.1* | *-138.7* | *-417.5* |
| | mixture | *syn* | 1.99044 | 1.98693 | 1.96977 | -118.1 | -142.5 | -424.5 |
| | | *anti* | 1.99045 | 1.98672 | 1.96943 | -114.3 | -141.5 | -421.3 |
| | | *average* | *1.99045* | *1.98677* | *1.96951* | *-115.2* | *-141.7* | *-422.0* |
| TPSSh | gas | *syn* | 1.99067 | 1.98839 | 1.96894 | -150.3 | -167.4 | -461.8 |
| | | *anti* | 1.99068 | 1.98824 | 1.96877 | -146.2 | -166.8 | -458.7 |
| | | *average* | *1.99068* | *1.98826* | *1.96879* | *-146.7* | *-166.9* | *-459.0* |
| | toluene | *syn* | 1.99046 | 1.98787 | 1.96989 | -140.8 | -160.3 | -453.4 |
| | | *anti* | 1.99047 | 1.98771 | 1.96964 | -137.4 | -159.9 | -450.8 |
| | | *average* | *1.99047* | *1.98773* | *1.96967* | *-137.9* | *-160.0* | *-451.1* |
| | $CH_2Cl_2$ | *syn* | 1.99012 | 1.98695 | 1.97118 | -127.5 | -151.4 | -441.6 |
| | | *anti* | 1.99010 | 1.98679 | 1.97090 | -124.4 | -150.4 | -439.0 |
| | | *average* | *1.99010* | *1.98683* | *1.97097* | *-125.1* | *-150.7* | *-439.6* |
| | mixture | *syn* | 1.99029 | 1.98739 | 1.97071 | -132.6 | -154.4 | -446.1 |
| | | *anti* | 1.99030 | 1.98724 | 1.97041 | -129.6 | -153.8 | -443.8 |
| | | *average* | *1.99030* | *1.98728* | *1.97048* | *-130.3* | *-154.0* | *-444.3* |

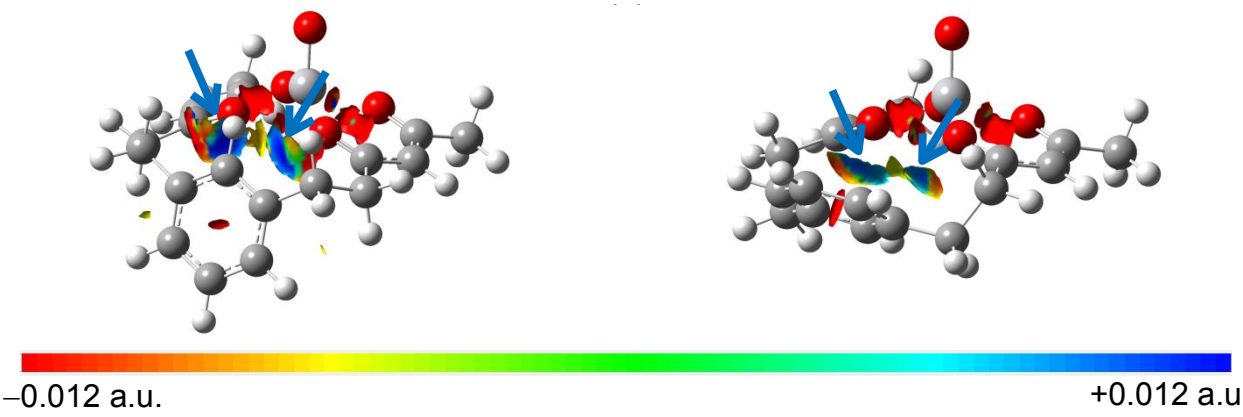


**Figure S26.** Intra-complex Non-Covalent Interactions (NCIs) in *anti*- (left) and *syn*-[(VO)(bdhb)] (right) conformers, depicted using the product of the sign of the second largest eigenvalue of electron density Hessian matrix and electron density, mapped on the reduced density gradient (RDG), with an isovalue $s$ = ½. The blue arrows indicate attractive intra-complex NCIs established between the two β-diketonato O atoms closer to the phenyl ring and two C atoms of the phenyl ring (blue regions).

## References


(1) *TopSpin 4.3.0*; Bruker AXS Inc.: Madison, WI, USA, 2023.

(2) Bachmann, S.; Neufeld, R.; Dzemski, M.; Stalke, D. New External Calibration Curves (ECCs) for the Estimation of Molecular Weights in Various Common NMR Solvents. *Chem. Eur. J.* **2016**, *22* (25), 8462–8465. https://doi.org/10.1002/chem.201601145.

(3) Crockett, M. P.; Zhang, H.; Thomas, C. M.; Byers, J. A. Adding Diffusion Ordered NMR Spectroscopy (DOSY) to the Arsenal for Characterizing Paramagnetic Complexes. *Chem. Commun.* **2019**, *55* (96), 14426–14429. https://doi.org/10.1039/C9CC08229H.

(4) Spek, A. L. PLATON SQUEEZE: A Tool for the Calculation of the Disordered Solvent Contribution to the Calculated Structure Factors. *Acta Crystallogr. Sect. C Struct. Chem.* **2015**, *71* (1), 9–18. https://doi.org/10.1107/S2053229614024929.

(5) Macrae, C. F.; Sovago, I.; Cottrell, S. J.; Galek, P. T. A.; McCabe, P.; Pidcock, E.; Platings, M.; Shields, G. P.; Stevens, J. S.; Towler, M.; Wood, P. A. Mercury 4.0 : From Visualization to Analysis, Design and Prediction. *J. Appl. Crystallogr.* **2020**, *53* (1), 226–235. https://doi.org/10.1107/S1600576719014092.

(6) Farrugia, L. J. WinGX and ORTEP for Windows: An Update. *J. Appl. Crystallogr.* **2012**, *45* (4), 849–854. https://doi.org/10.1107/S0021889812029111.